

An XYZ Parallel-Kinematic Flexure Mechanism With Geometrically Decoupled Degrees of Freedom

Shorya Awtar

John Ustick

Shiladitya Sen

Precision Systems Design Laboratory,
Mechanical Engineering,
University of Michigan,
Ann Arbor, MI 48109

A novel parallel-kinematic flexure mechanism that provides highly decoupled motions along the three translational directions (X, Y, and Z) and high stiffness along the three rotational directions (θ_x , θ_y , and θ_z) is presented. Geometric decoupling ensures large motion range along each translational direction and enables integration with large-stroke ground-mounted linear actuators or generators, depending on the application. The proposed design, which is based on a systematic arrangement of multiple rigid stages and parallelogram flexure modules, is analyzed via nonlinear finite elements analysis (FEA). A proof-of-concept prototype is fabricated to validate the predicted large range and decoupled motion capabilities. The analysis and the hardware prototype demonstrate an XYZ motion range of $10\text{ mm} \times 10\text{ mm} \times 10\text{ mm}$. Over this motion range, the nonlinear FEA predicts cross-axis errors of less than 7.8%, parasitic rotations less than 10.8 mrad, less than 14.4% lost motion, actuator isolation better than 1.5%, and no perceptible motion direction stiffness variation.
[DOI: 10.1115/1.4007768]

1 Introduction and Motivation

Flexure mechanisms derive motion from elastic deformation instead of employing traditional sliding or rolling interfaces [1,2]. This joint-less construction entirely eliminates friction, wear, and backlash, leading to highly repeatable motion [3]. Further benefits include design simplicity, zero assembly and maintenance, and potentially infinite life.

As a result of these attributes, flexure mechanisms are widely employed in various design applications. In particular, *multi-axis* flexure mechanisms are used in precision alignment and actuation instruments, MEMS sensors and actuators, energy harvesting devices, micro and nanomanipulators, high dexterity medical devices, scanning probe systems for precision metrology and nanomanufacturing, as well as consumer products [4].

Multi-axis, or multiple degrees of freedom (DoF), functionality may be achieved either via a serial kinematic [5,6] configuration or a parallel-kinematic [7–9] configuration. While a serial kinematic design may be simply conceived by stacking one single-axis system on top of another until the desired degrees of freedom are achieved, this construction is often large and bulky. Moreover, moving cables and actuators adversely affect dynamic performance. Parallel-kinematic designs, on the other hand, employ ground-mounted actuators and are often compact and simple in construction. Compared to serial kinematic designs, their main drawbacks include smaller motion range, potential for overconstraint, and greater error motions. Parallel-kinematic designs are

also not obvious in their conception and therefore present a nontrivial design problem.

The objective of this paper is to overcome the above-mentioned traditional drawbacks in the design of an XYZ parallel-kinematic flexure mechanism. The proposed concept is inherently free of geometric overconstraints, resulting in large translational motions along the X, Y, and Z directions, and exhibits small error motions (cross-axis errors and parasitic rotations). Large motion range along multiple axes is critical in many of the above applications, particularly nanopositioning and kinetic energy harvesting, which provide the primary motivation for this work.

Nanopositioning systems are macroscale mechatronic motion systems capable of nanometric precision, accuracy, and resolution [10], and are therefore vital to scanning probe based microscopy, manipulation, and manufacturing [11,12]. Given their lack of friction and backlash, flexure mechanisms are the most common bearing choice for nanopositioning systems. However, most existing flexure-based multi-axis nanopositioning systems are limited to approximately $100\ \mu\text{m}$ motion range per axis (see prior art in Sec. 2). To broaden the impact of scanning probe techniques in nanometrology and nanolithography, there is a need to increase this motion range by several folds [13–15]. The challenge here lies not only in creating a multi-axis flexure mechanism that is capable of large motion range but also in the mechanical integration of the flexure mechanism with ground-mounted actuators.

Since flexure mechanisms exhibit the motion guidance attributes of mechanisms as well as the elastic attributes of structures, they are also highly suited for energy harvesting schemes based on a resonant proof mass subject to cyclic inertial loads. Even though the excitation, and therefore the available energy, is generally in multiple directions, most energy harvesting devices employ single-axis resonators [16]. Given the fact that the energy harvested is directly proportional to the amplitude of oscillation [17], multi-axis flexure mechanisms with large motion range are promising for efficient kinetic energy harvesting. However, in addition to providing large motion range in each direction, any candidate flexure mechanism also has to interface with fixed-axis generators for mechanical to electrical energy conversion.

In both the above applications, a motion range of several millimeters per axis would be desirable in a macroscale construction. This paper covers the conception, FEA, and preliminary hardware validation of an XYZ parallel-kinematic flexure mechanism (Fig. 1) that meets the large motion range requirement as well as the pertinent actuator/generator integration challenges associated with these applications. Section 2 describes these design challenges in addition to providing a brief overview of the existing literature on XYZ flexure mechanisms. Section 3 presents the proposed XYZ flexure mechanism design along with a detailed description of its motion characteristics and a proof-of-concept hardware prototype.

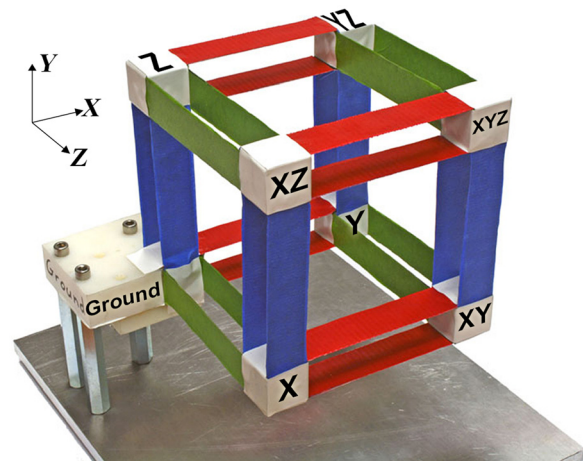


Fig. 1 Proposed XYZ flexure mechanism design

Contributed by the Mechanisms and Robotics Committee of ASME for publication in the JOURNAL OF MECHANISMS AND ROBOTICS. Manuscript received March 1, 2012; final manuscript received August 17, 2012; published online November 15, 2012. Assoc. Editor: Federico Thomas.

A comprehensive nonlinear FEA of this flexure mechanism is presented in Sec. 4. The predicted motion performance in terms of motion range, stiffness variation, cross-axis error, actuator isolation, lost motion, and parasitic rotations is reported. Conclusions and future work are summarized in Sec. 5.

2 Design Challenges and Prior Art Review

Motion range in multi-axis parallel-kinematic mechanisms is often restricted due to overconstraint, which can arise from a geometric layout that exhibits coupling between the motion axes. This ultimately leads to binding and restricts mobility. Thus, the motion axes—X, Y, and Z, in this case—must be sufficiently decoupled from each other so that motion in one axis does not affect or constrain motion in the other axes. Additionally, the undesired parasitic rotations (i.e., θ_x , θ_y , and θ_z) should be inherently restricted and minimized by the kinematics of the design. This eliminates the need for additional actuators, beyond the minimum three needed for X, Y, and Z actuations, to correct these undesired rotations. Moreover, in addition to providing geometric decoupling between the three motion axes, it is also important that the flexure mechanism addresses the geometric constraints associated with integrating practically available actuators or generators.

For an XYZ nanopositioning system, the use of linear actuators provides the greatest simplicity by avoiding any additional transmission. However, most linear actuators [18]—including voice coils, linear motors, piezoelectric stacks, and inchworm style actuators—produce motion along an “actuation axis,” defined by their geometry, and do not tolerate off-axis loads or displacements. Thus, for these actuators to be integrated with a multi-axis flexure mechanism in a nanopositioning system, it is critical that the point of actuation on the flexure mechanism be inherently constrained to move only along the direction of actuation. At the same time, this point of actuation should not be influenced by the actuation in other directions, and vice versa. This attribute is referred to as *actuator isolation* [19].

Similarly, most generators also have a fixed linear or rotary axis of motion, defined by their geometry, which is essential for effective mechanical to electrical energy conversion. This geometric requirement has to be accommodated in a parallel-kinematic flexure mechanism designed for multi-axis energy harvesting.

Existing systematic and deterministic methods for the design of parallel-kinematic flexure mechanisms [20–22] are limited to the study of motion between a ground and a motion stage, and do not address the additional geometric constraints associated with transducers. Also, many of these existing approaches do not recognize the benefits of elastic averaging in flexure mechanisms, which can be leveraged to generate highly symmetric designs [21,23]. Consequently, most existing parallel-kinematic designs are based on qualitative arguments and rationale; a sampling of these designs is presented next.

Several desktop-size parallel-kinematic XYZ flexure mechanisms have been reported in the literature, but none provide the desired large motion range capability (~ 10 mm per axis). While some of these designs are true parallel-kinematic arrangements, others represent a hybrid arrangement comprising a parallel connection of multiple serial kinematic chains.

In the former category, Davies [7] reports a three-DoF (XYZ) as well as a full six-DoF parallel-kinematic design, with a sub-millimeter range per translational axis. Culpepper and Anderson [24] present a planar monolithic six-DoF compliant structure with a stroke of $100\ \mu\text{m}$ per translational axis. Dagalakis and Amatucci [8] offer a six-DoF hexapod type parallel-kinematic design with improved actuator isolation. A six-DoF parallel-kinematic stage is reported by Yamakawa et al. [25] which provides a $100\ \mu\text{m}$ range in the X and Y directions, and $10\ \mu\text{m}$ in the Z direction. Yet another XYZ design, with $140\ \mu\text{m}$ range per axis, is presented by Li and Xu [26]. In all these cases, the motion range in each

direction is primarily restricted due to inadequate geometric decoupling and/or actuator isolation between the multiple axes.

In the hybrid category, Yao et al. [9] use a parallel connection of three serial kinematic chains, each comprising two four-bar parallelogram flexure mechanisms, to obtain X, Y, and Z motions ($85\ \mu\text{m}$ per axis) without any rotation. Arai et al. [27] also present a spatial arrangement to achieve XYZ motion capability. Actuated by piezoelectric stacks, a motion range of $20\ \mu\text{m}$ is reported. Similarly, Xueyen and Chen [28] employ a 3-PPP parallel mechanism to achieve good geometric decoupling and actuator isolation between the three motion directions. An overall motion range of 1 mm per axis is experimentally demonstrated. Another decoupled XYZ flexure mechanism design is conceptually proposed by Hao and Kong [29]. Here each of the three kinematic chains, which are connected in parallel, is individually a serial-parallel hybrid arrangement. While all these designs appropriately address the issues of geometric coupling and actuator isolation, their hybrid serial-parallel construction leads to a relatively bulky and complex construction.

Apart from these macroscale designs, several of multi-axis MEMS designs have also been reported for applications in inertial sensing and micro/nanomanipulation [30–34]. In this case, the designs and their associated performance are often dictated by the fundamentally planar nature of microfabrication. Given their small size, these designs generally exhibit a motion range of less than $10\ \mu\text{m}$ per axis. However, the focus in this paper is primarily on macroscale devices and applications where spatial geometries are relevant and beneficial.

3 Proposed XYZ Flexure Mechanism Design

In this section, we first present a parallel-kinematic constraint map that overcomes the above-listed challenges and inherently (i) provides geometric decoupling between the X, Y, and Z motion axes, (ii) constrains motion along the three rotational directions, and (iii) allows actuator/generator integration along each translational direction. This constraint map serves as the basis for the synthesis of a novel, compact, parallel-kinematic XYZ flexure mechanism design that embodies the above desired attributes.

The proposed constraint map is shown in Fig. 2, and comprises two kinds of building blocks—rigid stages represented by the blocks and constraint elements represented by the colored connectors. The rigid stages are labeled as Ground, X stage, Y stage, Z stage, XY stage, YZ stage, ZX stage, and XYZ stage. This nomenclature is based on the primary mobility of any given stage—the X stage is constrained such that it has mobility along the X direction only, the XY stage is constrained such that it has mobility in the X and Y directions only, the XYZ stage is constrained such that it has mobility in the X, Y, and Z directions, and so on. In the subsequent paragraphs, we will describe how such mobility and constraint characteristics are achieved.

In addition to the rigid stages, there are constraint elements classified by color—green, blue, and red (see color in on-line

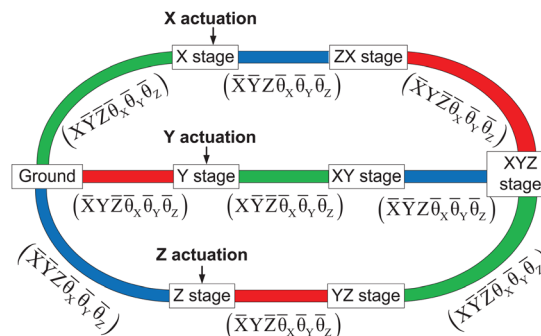


Fig. 2 Proposed constraint map for parallel-kinematic XYZ flexure mechanism synthesis (color in online version)

version). The green constraint elements allow motion in the X direction only and constrain all other motions ($\bar{X}\bar{Y}\bar{Z}\bar{\theta}_X\bar{\theta}_Y\bar{\theta}_Z$); the red constraint elements allow motion in the X direction only and constrain all other motions ($\bar{X}\bar{Y}\bar{Z}\bar{\theta}_X\bar{\theta}_Y\bar{\theta}_Z$); and, the blue constraint elements allow motion in the X direction only and constrain all other motions ($\bar{X}\bar{Y}\bar{Z}\bar{\theta}_X\bar{\theta}_Y\bar{\theta}_Z$).

Next, we describe the rationale behind this constraint map. For a three DoF parallel-kinematic mechanism, there have to be three parallel connecting paths between Ground and the XYZ stage—one each for the X, Y, and Z directions. Each path should have the following characteristics:

- (1) There should be an actuation stage that is constrained to move in one translational direction only.
- (2) The translational motion of this actuation stage should be entirely transmitted to the XYZ Stage, without restricting the motion of the XYZ Stage in the other two translational directions.
- (3) Rotational motions of the XYZ Stage should be constrained.

Thus, the X stage is connected to Ground via a ($\bar{X}\bar{Y}\bar{Z}\bar{\theta}_X\bar{\theta}_Y\bar{\theta}_Z$) constraint that allows an X actuator to be integrated at this location. In order to transmit the resulting X translation of the X stage to the XYZ stage, while permitting relative Y and Z translations, these two stages should be connected via a ($\bar{X}\bar{Y}\bar{Z}\bar{\theta}_X\bar{\theta}_Y\bar{\theta}_Z$) constraint. In other words, the connection between the X and XYZ stages should allow only Y and Z DoF, and constrain all others. This can be accomplished by connecting a ($\bar{X}\bar{Y}\bar{Z}\bar{\theta}_X\bar{\theta}_Y\bar{\theta}_Z$) constraint and a ($\bar{X}\bar{Y}\bar{Z}\bar{\theta}_X\bar{\theta}_Y\bar{\theta}_Z$) constraint in series, as shown in Fig. 2.

An analogous rationale is followed along the Y and Z actuation paths to complete the constraint map. The fact that each path provides actuation in one direction only without affecting the other two directions provides the desired geometric decoupling. The resulting constraint map provides the basis for generating flexure mechanism topologies that inherently provide large, unconstrained translations in the X, Y, and Z directions, and restricted rotations.

To generate a physical flexure mechanism embodiment, we populate the constraint map of Fig. 2 with the parallelogram flexure module (PFM), which serves as an effective single translational DoF constraint element. The resulting flexure mechanism is shown in Fig. 3. The rigid stages are all colored white, and the PFMs are colored green, blue, and red (color in online version), according to Fig. 2. The green PFMs deform primarily in the X direction and remain stiff in all other directions; the red PFMs deform primarily in the Y direction and remain stiff in all other directions; and, the blue PFMs deform primarily in the Z direction and exhibit high stiffness in all other directions.

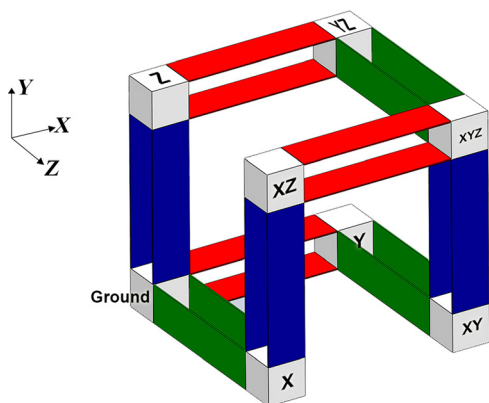
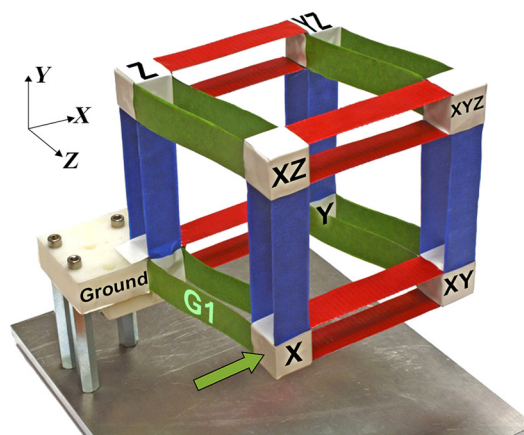
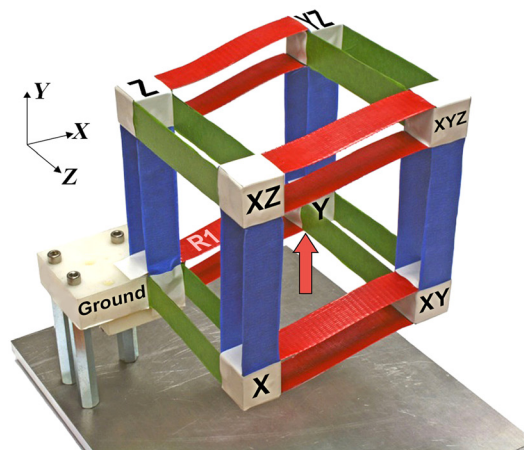


Fig. 3 Flexure mechanism concept based on constraint map (color in online version)

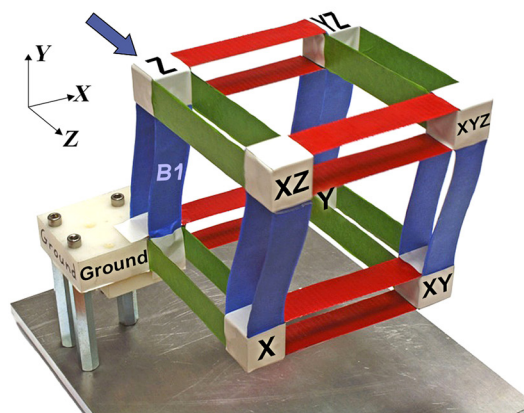
It is important to recognize that neither the constraint map of Fig. 2 nor the embodiment of Fig. 3 follow the principles of “exact constraint” design [20]. For example, the rotations of the rigid stages are overconstrained, which actually helps reduce these undesired rotations. The embodiment of Fig. 3 may be further augmented by incorporating additional PFMs that serve as non-conflicting constraint elements to yield the highly symmetric, cubic flexure mechanism embodiment shown in Fig. 4. The enhanced symmetry resulting from this intentional use of



(a)



(b)



(c)

Fig. 4 Proposed flexure mechanism design: (a) X motion only, (b) Y motion only, and (c) Z motion only (color in online version)

overconstraint further reduces the stage rotations and cross-axis errors, while retaining the geometric decoupling and actuator isolation provided by the original constraint map of Fig. 2. The distributed compliance of the PFMs enables “elastic averaging” [23], which makes the overall design more tolerant to manufacturing and assembly errors in spite of the overconstraint.

In this parallel-kinematic flexure mechanism, the X stage is constrained to move primarily along the X direction guided by the green PFM labeled G1, as shown in Fig. 4(a). Because of the high stiffness of the blue and red PFMs in the X (color in online version) direction, the X displacement of this X stage is passed on to the XY, XZ, and the XYZ stages. But at the same time, the XY and XYZ stages remain free to move in the Y direction because of the compliance of the red PFMs, and the XZ and XYZ stages remain free to move in the Z direction because of the compliance of the blue PFMs.

Similarly, the Y stage is constrained to move primarily along the Y direction because of PFM R1, as seen in Fig. 4(b) (color in online version). This Y displacement of the Y stage is transmitted to the XY, YZ, and XYZ stages because of the high stiffness of the green and blue PFMs in the Y direction. But at the same time, the XY and XYZ stages remain free to move in the X direction because of the compliance of the green PFMs, and the YZ and XYZ stages remain free to move in the Z direction because of the compliance of the blue PFMs.

Finally, the Z stage is constrained to move primarily along the Z direction because of PFM B1 (Fig. 4(c)) (color in online version). This Z displacement of the Z stage is transmitted to the YZ, XZ, and XYZ stages because of the high stiffness of the green and red PFMs in the Z direction. But at the same time, the XZ and XYZ stages remain free to move the X direction because of the compliance of the green PFMs, and the YZ and XYZ stages remain free to move in the Y direction because of the compliance of the red PFMs. The completely analogous behavior of each of the X, Y, and Z axes, with respect to the other two, highlights the geometric symmetry of this design.

Thus, while the X stage is constrained to move primarily along the X direction, its motion does not influence the Y and Z stages. Due to symmetry, the same holds true for the Y stage and the Z stage. This provides the desired actuator/generator isolation between the three directions. A video demonstration of the overall motion characteristics of this XYZ flexure mechanism may be viewed in Ref. [35].

Furthermore, the proposed parallel-kinematic flexure design behaves like a mechanical summation device—the X motion of the X stage, the Y motion of the Y stage, and the Z motion of the Z stage are all combined and exhibited at the XYZ stage. In a multi-axis nanopositioning system, large-stroke fixed-axis linear actuators would be mounted at the X, Y, and Z stages, and the XYZ stage would serve as the motion stage with three DoF. In the context of multi-axis energy harvesting, this flexure mechanism would serve as a mechanical separator. Any arbitrary combination of the X, Y, and Z motions of the XYZ stage, which would serve as a proof mass in this case, would be mechanically separated into an X motion only at the X stage, a Y motion only at the Y stage, and a Z motion only at the Z stage. These single-axis motions could then be efficiently harvested using large-stroke fixed-axis linear generators.

The constraint map of Fig. 2 can also be populated using other single translational DoF flexure modules, such as the multibeam parallelogram, the double parallelogram, etc. This would result in different XYZ flexure mechanism embodiments, but with the same geometric decoupling and actuator isolation behavior as seen above. However, more detailed motion performance, such as error motions, stiffness variations, and dynamic behavior, would be different for each. In fact, if the constraint elements were ideal, i.e., exhibiting zero stiffness in their DoF direction, and infinite stiffness and zero motions in their constrained directions, the resulting XYZ flexure mechanism would also be ideal—zero stiffness in the X, Y, and Z directions, zero parasitic rotations of all

the stages, perfect decoupling between the motion axes, perfect actuator isolation, zero lost motion between the point of actuation and the main motion stage, etc. However, in reality, any flexure module that is used as a constraint element is not ideal [36]. This gives rise to small but finite deviations from the ideal motion behavior in any XYZ flexure mechanism resulting from the above constraint map.

A primitive variation of such a parallel-kinematic XYZ flexure design has been proposed in the past [37], but without proper constraint-based rationale for topological layout. This resulted in significantly compromised performance in terms of stage rotations, actuator isolation, and lost motion.

The proof-of-concept prototype shown in Figs. 1 and 4 was fabricated to validate the above claims of unconstrained, decoupled, and large motions along the X, Y, and Z directions as well as actuator/generator isolation. The overall size, detailed dimensions, and material selection were selected to provide a ± 5 mm motion range (Δ) per axis while ensuring adequate safety factor ($\eta = 3$) against material yielding. Given the geometry and constraint pattern of the proposed design, it is evident that the constituent beam flexures deform predominantly in an S-shape. For this deformation, the maximum allowable end deflection of an individual beam before the onset of yielding is given by [37]

$$\Delta = \frac{1}{3} \cdot \frac{1}{\eta} \cdot \left(\frac{S_y}{E} \right) \cdot \left(\frac{L^2}{T} \right)$$

where S_y is the yield strength, E is the Young's modulus, T is the beam thickness, and L is the beam length. For the material, Aluminum 6061 was chosen because of its overall good flexural properties and machinability. With this material choice, the desired motion range and safety factor were achieved with $L = 101.6$ mm (4 in.) and $T = 0.762$ mm (0.030 in.). The beam depth was chosen to be 25.4 mm (1 in.), a standard plate stock, to minimize the stage rotations. This resulted in a center-to-center beam spacing of 24.64 mm for each PFM, and a 25.4 mm \times 25.4 mm size for each of the rigid stages. Standard machining and assembly methods were employed to fabricate the prototype.

While the expected motion behavior of the XYZ flexure mechanism design was qualitatively validated by this simple hardware prototype, as seen in Fig. 4, assessment of the small deviations from ideal motion behavior requires more detailed analysis, which is covered next. Of particular interest are motion direction stiffness and variation, cross-axis errors, transmission stiffness variation, lost motion, actuator isolation, and parasitic rotations.

4 Prediction of Motion Performance via Finite Elements Analysis

Predicting the detailed motion performance of large range flexure mechanisms requires a nonlinear force–displacement analysis, as shown previously [19,36]. Ideally, a closed-form nonlinear analysis is preferable since it offers quantitative and parametric insights into the relation between the mechanism's geometry and its motion performance. However, such an analysis entails considerable mathematical complexity and is the subject of our ongoing and future work. Instead, to expediently obtain early validation and assessment of the proposed design, we conducted nonlinear FEA using ANSYS.

Each beam in the flexure mechanism is modeled using square-shaped SHELL181 elements, with the large displacement option (NLGEOM) turned on to capture geometric nonlinearities and cross-sectional warping. Additionally, this element accurately models the finite stress along width of the beam, and the Wagner effects that play an important role in the torsion of thin, wide beams [38,39]. To determine an optimal mesh density, a convergence test is conducted between end displacements and mesh size. A 64×16 mesh of square elements per beam is chosen to provide better than 0.25% convergence with respect to mesh size [39].

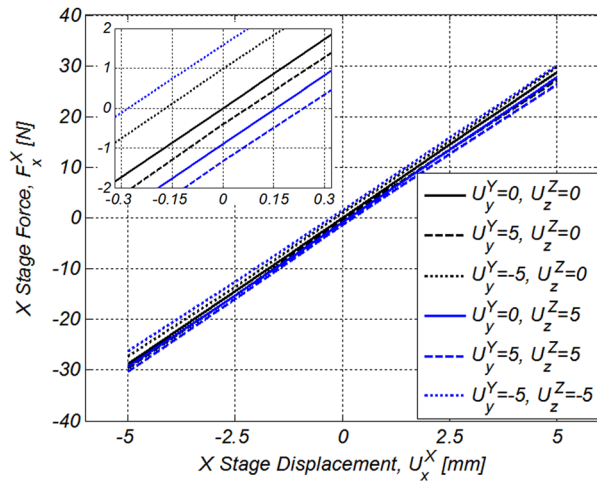


Fig. 5 X direction force–displacement relation

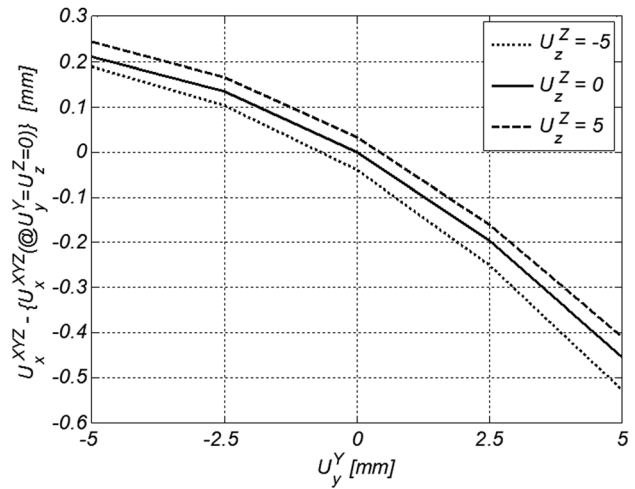


Fig. 7 X direction cross-axis error motion

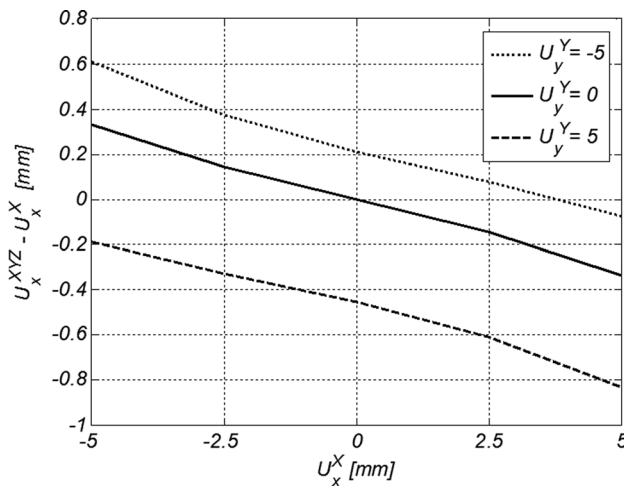


Fig. 6 X direction lost motion

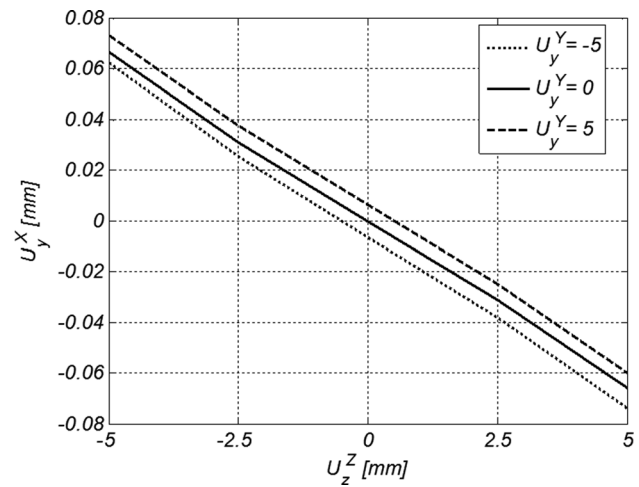


Fig. 8 X actuator isolation (Y direction)

The corner stages are modeled using the MPC184 rigid elements. Standard material properties for Aluminum 6061 are assumed ($E = 68,900 \text{ N mm}^{-2}$ and $\nu = 0.33$). The displacement in each direction is varied over a range of -5 mm to $+5 \text{ mm}$ in five equal increments, resulting in a total of 125 loading conditions that are analyzed. While reporting the FEA results in the following paragraphs and figures, we follow a nomenclature in which the superscript represents the rigid stage being considered and the subscript represents the relevant direction of displacement, rotation, or force associated with this stage. For example, U_x^Y represents the X direction displacement of the Y stage, θ_y^Z represents the Y direction rotation of the Z stage, F_z^X represents the Z direction force on the X stage, and so on.

Figure 5 illustrates the geometric decoupling between the X, Y, and Z motion directions in the proposed design. The X direction force applied at the X stage (F_x^X) is plotted versus the X direction displacement of the X stage (U_x^X), for various combinations of Y and Z actuations (U_y^Y and U_z^Z). The resulting X direction stiffness not only remains constant over the entire X direction motion range but it is also insensitive to actuation in the Y and Z directions. The small shifts in the force–displacement line (inset) in the presence of U_y^Y and U_z^Z are due to small cross-axis errors that are characterized further below. Although not plotted here, the Y and Z direction stiffnesses also exhibit a similar behavior because of the symmetric design. This validates the unique attribute of the

proposed flexure mechanism that its mobility in one direction is not influenced by motion in the other directions. This decoupling allows large motions in each direction, unconstrained by the geometry and limited only by material failure.

Figure 6 captures the X direction motion that is “lost” between the point of actuation and the point of interest. This difference between U_x^{XYZ} and U_x^X is plotted over the entire range of X actuation for different values of the Y actuation (U_y^Y). Because this lost motion is found to be largely insensitive to the Z actuation (U_z^Z), the curves in Fig. 6 are plotted for $U_z^Z = 0 \text{ mm}$ only. The X direction lost motion varies from 0.6 mm , when U_x^X and U_y^Y are both -5 mm to -0.84 mm when U_x^X and U_y^Y are both 5 mm . Lost motion is also inversely related to the transmission stiffness, which represents the stiffness between the point of actuation and the point of interest and is critical in high speed motion control applications.

Next, the cross-axis error, which represents any motion of the XYZ stage in one direction caused by actuation in a different direction, is illustrated in Fig. 7. This error in X direction is mathematically given by the difference between the actual X displacement of the XYZ stage (U_x^{XYZ}) in the presence of Y and Z actuations (U_y^Y and U_z^Z) and the nominal X displacement of the XYZ stage (U_x^{XYZ}) in the absence of Y and Z actuations. Thus, $U_x^{XYZ} - \{U_x^{XYZ} (@U_y^Y = U_z^Z = 0)\}$ is plotted over the entire range of U_y^Y for three values of U_z^Z . Since this error motion is

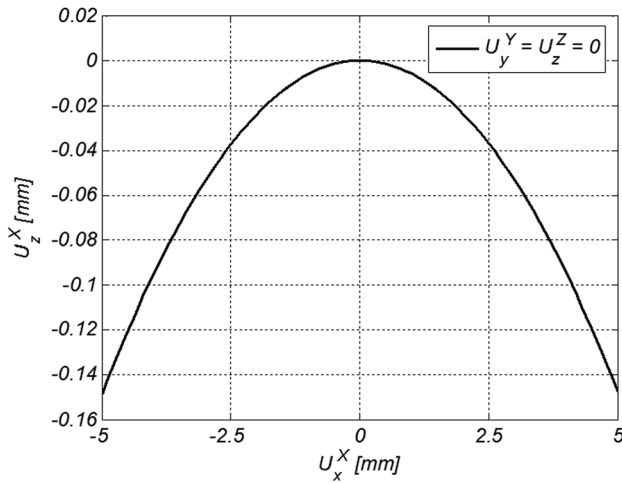


Fig. 9 X actuator isolation (Z direction)

found to be largely insensitive to X actuation (U_x^X), the curves in Fig. 7 are plotted for $U_x^X = 0$ mm only. The cross-axis error motion in X direction varies from a maximum value of 0.25 mm when U_y^Y is -5 mm and U_z^Z is 5 mm to -0.53 mm when U_y^Y is 5 mm and $-U_z^Z$ is 5 mm. The same trend is observed for the Y and Z direction cross-axis errors.

Actuator isolation in a multi-axis flexure mechanism ensures that the point of actuation in any given direction moves only in that direction and is not influenced by actuation in the other directions. Figures 8 and 9 show the Y and Z direction displacements of the X stage, U_y^X and U_z^X , respectively. For different values of Y actuation (U_y^Y), the Y direction displacement of the X stage (U_y^X) is plotted over the entire range of Z actuation (U_z^Z) in Fig. 8. Since this motion is found to be largely insensitive to X actuation, the curves are plotted for $U_x^X = 0$ mm only. The maximum Y direction motion of the X stage is 0.073 mm when U_y^Y is 5 mm and U_z^Z is -5 mm, and -0.073 mm when U_y^Y is -5 mm and U_z^Z is 5 mm.

Figure 9 shows the Z direction displacement of the X stage (U_z^X) over the entire range of X actuation (U_x^X). Since this motion is found to be largely insensitive to both Y and Z actuations, the curve is plotted for Y and Z actuations held at 0 mm. The maximum Z direction motion of the X stage is -0.148 mm when U_x^X is ± 5 mm.

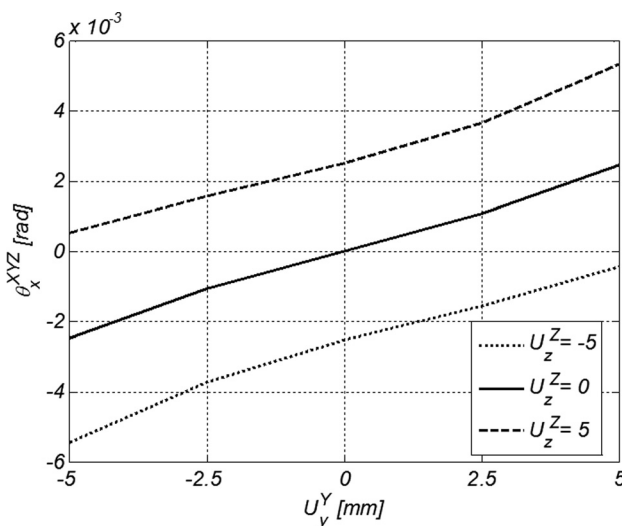


Fig. 10 X direction rotation of the XYZ stage

In an XYZ flexure mechanism, all rotations are undesired and represent parasitic errors. Figure 10 shows the XYZ stage rotations about the X direction (θ_x^{XYZ}) over the entire range of Y actuation for three different Z actuations. Since this rotation is found to be largely insensitive to X actuation (U_x^X), the curves are plotted for U_x^X held at 0 mm. The maximum X direction rotation of the XYZ stage varies between a maximum positive value of 5.4 mrad when U_y^Y and U_z^Z are both 5 mm to a maximum negative value of -5.4 mrad when U_y^Y and U_z^Z are both -5 mm. Because of design symmetry, the XYZ stage rotation about the Y direction (θ_y^{XYZ}) depends similarly on the X and Z actuations but not as much on the Y actuation. And, the XYZ stage rotation about the Z direction (θ_z^{XYZ}) depends on the X and Y actuations but not as much on the Z actuation.

Below, we summarize the FEA based motion performance of the proposed XYZ flexure mechanism, with the chosen dimensions

- (i) 10 mm motion range in each direction, with the stiffness remaining invariant with actuation along the other two directions.
- (ii) Lost motion per axis less than 1.44 mm over the entire motion range ($<14.4\%$ of range).
- (iii) Cross-axis error less than 0.78 mm over the entire motion range ($<7.8\%$ of range).
- (iv) Actuator isolation less than 0.15 mm in any given direction over the entire motion range ($<1.5\%$ of range).
- (v) Parasitic rotations of the XYZ stage less than 10.8 mrad over the entire motion range.

These FEA results also help highlight the extent of nonlinear behavior in the mechanics of the proposed flexure mechanism design. However, final validation of the performance attributes of the proposed XYZ flexure design can only come from quantitative experimental measurements, which are part of our ongoing and future research.

5 Conclusion

This paper presents a novel, compact, and symmetric XYZ parallel-kinematic flexure mechanism that provides highly decoupled motion along the three translational directions, inherently minimizes error motions, and accommodates large-stroke single-axis actuators/generators. These claims have been quantitatively validated via finite element analysis and physically demonstrated by means of a proof-of-concept prototype.

Ongoing research efforts include a closed-form nonlinear analysis of this flexure mechanism to gain greater design insight and to enable a parametric design optimization of its motion performance (e.g., maximize motion range, minimize error motions, etc.) for applications in nanositioning. A more refined hardware prototype and associated metrology setup are currently being fabricated to experimentally measure the predicted motion direction stiffness, cross-axis error, lost motion, actuator isolation, and parasitic rotations. Furthermore, given the significance of structural dynamics in nanositioning as well as energy harvesting applications, a systematic dynamic modeling is also being conducted.

Acknowledgment

This research was supported in part by the National Science Foundation grants CMMI-0846738 and CMMI-1100807.

References

- [1] Jones, R. V., 1962, "Some Uses of Elasticity in Instrument Design," *J. Sci. Instrum.*, **39**, pp. 193–203.
- [2] Smith, S. T., 2000, *Flexures: Elements of Elastic Mechanisms*, Gordon and Breach Science Publishers, New York.

- [3] Slocum, A. H., 1992, *Precision Machine Design*, Society of Manufacturing Engineers, Dearborn, MI.
- [4] Awtar, S., Ustick, J., and Sen, S., 2011, "An XYZ Parallel Kinematic Flexure Mechanism With Geometrically Decoupled Degrees of Freedom," Proceedings of ASME IDETC/CIE, Washington DC, Paper No. 47713.
- [5] Fischer, F. L., 1981, "Symmetrical 3 DOF Compliance Structure," U.S. Patent No. 4,447,048.
- [6] Bednorz, J. G., Hollis, R. L., Jr., Lanz, M., Pohl, W. D., and Yeack-Scranton, C. E., 1985, "Piezoelectric XY Positioner," U.S. Patent No. 4,520,570.
- [7] Davies, P. A., 2001, "Positioning Mechanism," U.S. Patent No. 6,193,226.
- [8] Dagalakis, N. G., and Amatucci, E., 2001, "Kinematic Modeling of a 6 Degree of Freedom Tri-Stage Micro-Positioner," Proceedings of ASPE 16th Annual Meeting, Crystal City, VA.
- [9] Yao, Q., Dong, J., and Ferreira, P. M., 2008, "A Novel Parallel-Kinematics Mechanisms for Integrated, Multi-Axis Nanopositioning—Part 1: Kinematics and Design for Fabrication," *Precis. Eng.*, **32**(1), pp. 7–19.
- [10] Hicks, T. R., and Atherton, P. D., 1997, *The Nanopositioning Book*, Queensgate Instruments Ltd., Torquay, UK.
- [11] Devasia, S., Eleftheriou, E., and Moheimani, S. O. R., 2007, "A Survey of Control Issues in Nanopositioning," *IEEE Trans. Control Syst. Technol.*, **15**(5), pp. 802–823.
- [12] Jordan, S., and Lula, B., 2005, "Nanopositioning: The Technology and the Options," *The 2005 Photonics Handbook*, Laurin Publications, Pittsfield, MA.
- [13] Dai, G., Pohlenz, F., Danzebrink, H.-U., Xu, M., Hasche, K., and Wilkening, G., 2004, "Metrological Large Range Scanning Probe Microscope," *Rev. Sci. Instrum.*, **75**(4), pp. 962–969.
- [14] Sinno, A., Ruau, P., Chassagne, L., Topcu, S., and Alayli, Y., 2007, "Enlarged Atomic Force Microscopy Scanning Scope: Novel Sample-Holder Device With Millimeter Range," *Rev. Sci. Instrum.*, **78**(9), pp. 1–7.
- [15] Wouters, D., and Schubert, U. S., 2004, "Nanolithography and Nanochemistry: Probe-Related Patterning Techniques and Chemical Modification for Nanometer-Sized Devices," *Angew. Chem., Int. Ed.*, **43**(19), pp. 2480–2495.
- [16] Beeby, S., Tudor, M., and White, N., 2006, "Energy Harvesting Vibration Sources for Microsystems Applications," *Meas. Sci. Technol.*, **12**, pp. R175–R195.
- [17] Mitcheson, P. D., Rao, G. K., and Green, T. C., 2008, "Energy Harvesting From Human and Machine Motion for Wireless Electronic Devices," *Proc. IEEE*, **96**(9), pp. 1457–1486.
- [18] Smith, S. T., and Seugling, R. M., 2006, "Sensor and Actuator Considerations for Precision, Small Machines," *Precis. Eng.*, **30**(3), pp. 245–264.
- [19] Awtar, S., and Slocum, A. H., 2007, "Constraint-Based Design of Parallel Kinematic XY Flexure Mechanisms," *ASME J. Mech. Des.*, **129**(8), pp. 816–830.
- [20] Blanding, D. L., 1999, *Exact Constraint: Machine Design Using Kinematic Principles*, ASME Press, New York.
- [21] Hopkins, J. B., and Culpepper, M. L., 2010, "Synthesis of Multi-Degree of Freedom, Parallel Flexure System Concepts via Freedom and Constraint Topology (FACT)—Part I: Principles," *Precis. Eng.*, **34**(2), pp. 259–270.
- [22] Su, H.-J., and Tari, H., 2010, "Realizing Orthogonal Motions With Wire Flexures Connected in Parallel," *ASME J. Mech. Des.*, **132**(12), p. 121002.
- [23] Awtar, S., Shimotsu, K., and Sen, S., 2010, "Elastic Averaging in Flexure Mechanisms: A Three-Beam Parallelogram Flexure Case Study," *J. Mech. Rob.*, **2**(4), p. 041006.
- [24] Culpepper, M. L., and Anderson, G., 2004, "Design of a Low-Cost Nano-Manipulator Which Utilizes a Monolithic, Spatial Compliant Mechanism," *Precis. Eng.*, **28**(4), pp. 469–482.
- [25] Yamakawa, K., Furutani, K., and Mohri, N., 1999, "XYZ-Stage for Scanning Probe Microscope by Using Parallel Mechanism," Proceedings of ASME DETC.
- [26] Li, Y., and Xu, Q., 2005, "Kinematic Design of a Novel 3-DOF Compliant Parallel Manipulator for Nanomanipulation," Proceedings of 2005 IEEE/ASME International Conference on Advanced Intelligent Mechatronics, Monterey, CA.
- [27] Arai, T., Herve, J. M., and Tanikawa, T., 1996, "Development of 3 DOF Micro Finger," Proceedings of Intelligent Robots and Systems '96.
- [28] Tang, X., and Chen, I. M., 2006, "A Large-Displacement and Decoupled XYZ Flexure Parallel Mechanism for Micromanipulation," Proceedings of IEEE International Conference on Automation Science and Engineering.
- [29] Hao, G., and Kong, X., 2009, "A 3-DOF Translational Compliant Parallel Manipulator Based on Flexure Motion," Proceedings of ASME IDETC, Paper No. 49040.
- [30] Li, F., Wu, M. C., Choquette, K. D., and Crawford, M. H., 1997, "Self-Assembled Microactuated XYZ Stages for Optical Scanning and Alignment," Proceedings of Transducers '97, Chicago.
- [31] Ando, Y., 2004, "Development of Three-Dimensional Electrostatic Stages for Scanning Probe Microscope," *Sens. Actuators, A*, **114**(2–3), pp. 285–291.
- [32] Mcneil, A. C., Li, G., and Koury, D. N., 2005, "Single Proof Mass 3 Axis MEMS Transducer," U.S. Patent No. 6,936,492.
- [33] Xinyu, L., Kim, K., and Sun, Y., 2007, "A MEMS Stage for 3-Axis Nanopositioning," *J. Micromech. Microeng.*, **17**(9), pp. 1796–1802.
- [34] Sarkar, N., Geisberger, A., and Ellis, M. D., 2004, "Fully Released MEMS XYZ Flexure Stage With Integrated Capacitive Feedback," U.S. Patent No. 6,806,991.
- [35] XYZ Flexure Demonstration Video, <http://www-personal.umich.edu/~awtar/XYZ%20flexure%20video1.mp4>
- [36] Awtar, S., Slocum, A. H., and Sevincer, E., 2007, "Characteristics of Beam-Based Flexure Modules," *ASME J. Mech. Des.*, **129**(6), pp. 625–639.
- [37] Awtar, S., 2004, "Synthesis and Analysis of Parallel Kinematic XY Flexure Mechanisms," Sc.D. thesis, Massachusetts Institute of Technology, Cambridge, MA.
- [38] Trahair, N. S., 2011, "Wagner's Beam Cycle," Research Report No. R916, School of Civil Engineering, University of Sydney, NSW, Australia.
- [39] Sen, S., 2012, "Closed Form Analytical Models for Design of Flexure Elements and Mechanisms," Ph.D. thesis, University of Michigan, Ann Arbor, MI.